International Journal of Advances in Scientific Research and Engineering (ijasre)

E-ISSN : 2454-8006

DOI: 10.31695/IJASRE.2022.8.11.11

Volume 8, Issue 11
November - 2022

Modelling and Analysis of Dynamic Stability of Glass Reinforced Plastic Pipes Subjected to Fluid Flow

Obuh Raphael Empire[1], Sylvester O Edelugo[1, 2], Ibeagwu Onyebuchi Isreal[1], B. N Ugwu[3], O U Ude[3]

[1]Department of Mechanical Engineering, University of Nigeria, Nsukka, Nigeria

[2]Africa Center for Excellence, University of Nigeria

[3]Department of Mechanical/Production Engineering, Enugu State university of Science and Technology, Nigeria

ABSTRACT

In the past, almost every industry worldwide patronized iron and its alloys for every major industrial design, construction and other forms of work. However, with the advent of the Glass Reinforced Plastic (GRP) as accepted in the United Kingdom or the Fibre Reinforced Plastic as accepted in the United States, which was discovered in the nineteen thirty's (1930's), the Glass Reinforced Plastic (GRP) has become very versatile as it has become a household name in most industries globally .It has attained this height through the significant properties it possesses, which include its ability to transform into moulds of difficult and delicate shapes and sizes which iron and its alloy may not find easy to submit to. It brings a host of other benefits in the form of long term performance and reliability, ease of installation and the ability to withstand corrosion and tuberculation. A service life of more than thrice that of the ductile iron pipes to mention but a few. Ductile Iron pipes are used in most petrochemical industries where pipeline plays a very important role in transporting crude oil and gas. As the service duration increases, the pipe lines are affected by corrosion mechanism which can lead to fatal accident. Corrosion can occur at both the internal and external surface of the pipelines. In general, corrosion would cause metal loss which leads to reduction in pipeline thickness and consequently reduce its strength. It becomes necessary that the stability of the Glass Reinforced Plastic (GRP) pipes are carefully investigated especially in the event of high pressure turbulent flows. This is the thrust of this work. In the light of the above, ductile iron pipes and Glass Reinforced Plastics (GRP) pipes of the same thicknesses were investigated, some special characteristics such as the bursting pressures were calculated using Peter Barlow's formula. The ANSYS software was also used for model analysis and compare the stress profile under dynamic condition for both pipes. Also the cost of production of pipes, classification and the difficulties encountered during their installation processes were examined. The result indicated an overwhelming encouragement to use Glass Reinforced Plastic (GRP) pipes as substitutes to the traditional ductile iron and its alloys in view of the fact that Glass Reinforced Plastic (GRP) pipes withstand corrosion and tuberculation while saving the huge cost that would have been used for pigging

Keywords: GRP, Ductile iron, Dynamic stability, Bursting Pressure, Fluid Flow.

1. INTRODUCTION

Fluid transportation through the GRP pipes are preferable when compared to other forms of pipes because of its fantastic properties. Some of these properties include its ability to resist corrosion and tuberculation, was expensive to maintain, ease of installation, light in weight, possess low electrical and thermal conductivity, a service left of more than three times that ductile iron, the ability to melt into intricate and delicate shapes and sizes and also withstand pressure that ductile iron pipes can withstand [1-3]. The integrity of other pipe materials are being challenged because most of them cannot meet up the characteristics that is highlighted above concerning the GRP pipes. The GRP pipes achieves a strong physical and mechanical properties because it joins the most desirable properties of the constituent elements and jettisons the less essential ones [4]. Application of the GRP element has grown steadily during the last years; as they become extremely popular in different areas of industries. [5]. Following the current global trend, GRP stand as a suitable and most effective replacement for the ductile iron pipes and PVC pipes based on it material properties especially on the corrosion and erosion resistance [6]. although considerable work has been done on the dynamic stability of pipes and its related researches; but that relating to the GRP has not been completely explored [6, 16, 21-30]. Nimish et al [5] studied the stress analysis of Glass Reinforced Polymer (GRP) pipes. In view

of the increasing knowledge of failure mechanisms, improved damage predictability and pipe quality, GRP piping is increasingly being considered in the field of high pressure fluid transmission with pressurization in excess of several Mega-Pascals. Since the GRP material consists of several layers, the analysis of stresses developed in it is complicated. Therefore, as the initial approach towards the project, the stress analysis of steel pipes was performed using ANSYS, which was followed by a comparative study of steel and GRP pipes. Ahmed et al [15] conducted a numerical study to predict the failure of fibre reinforced polymer pipes produced by filament winding when subjected to pure internal pressure. The analysis is done using the last ply failure technique for a four layered pipe oriented anti-symmetrically [±Ø°]2. ANSYS Composite Prep Post (version 15) is used for analysis. Three different composites were examined in this study: E-glass fiber/epoxy, carbon fiber/epoxy and aramid fiber/epoxy. Numerical analysis was further validated through experimental data in case of E-glass fiber/epoxy composite. Comparison proves a good degree of correlation. The maximum burst pressure for the three types of material is realised at [±55°]2 compared to a minimum pressure at [±0°]2. Zhu et al [23] evaluated the theoretical and empirical solutions for the prediction of pipe burst pressure relative to a burst pressure database comprising more than 100 tests covering a variety of pipeline steel grades and pipe sizes. Solutions considered include three based on plasticity theory for the end-capped, thin-walled, defect-free line pipe subjected to internal pressure in terms of the Tresca, von Mises, and ZL (or Zhu-Leis) criteria, one based on a cylindrical instability stress (CIS) concept, and a large group of analytical and empirical models previously evaluated by Law and Bowie. Peter and Leonid [21] presented a methodology for the analysis of piping vibration state. The acoustic resonance of medium (steam or water) is considered as most probable source of flow-induced vibration. For analysis of piping vibration induced by steady-state processes in a transmitted medium the mathematical model and corresponding computer code NETPULS were developed for evaluation of an acoustic oscillation in a liquid or gaseous medium. NETPULS is based on linearized mathematical model of quasi-stationary acoustic oscillation in the compressed medium. Mathematical model of this process takes into account influence of non-linear damping due to hydraulic friction and local hydraulic losses. The amplitude-frequency and phase-frequency characteristics of the gas-dynamic forces acting upon the piping discontinuities (bends, tees, branches etc.) were defined. The output obtained by NETPULS was used as input data for consequent calculation of mechanical vibrations of pipelines and evaluation of effectiveness of damping devices.

Fuping et al [24] conducted a series of plate impact shock-reshock and shock-release experiments to study the critical shear strength of a S2 glass fiber reinforced polymer –GRP composite under shock compression levels ranging from 0.8 to 1.8 GPa. The GRP was fabricated at ARL, Aberdeen, using S2 glass woven roving in a Cycom 4102 polyester resin matrix. The experiments were conducted by using an 82.5 mm bore single-stage gas gun at Case Western Reserve University. In order to conduct shock-reshock and shock-release experiments a dual flyer plate assembly was utilized. The shock-reshock experiments were conducted by using a projectile faced with GRP and backed with a relatively high shock impedance Al 6061-T6 plate; while for the shock-release experiments the GRP was backed by a relatively lower impedance polymethylmethacrylate backup flyer plate. A multi-beam velocity interferometer was used to measure the particle velocity profile at the rear surface of the target plate. Shun-Hu et al [25]developed an analytical solution of burst pressure for pipe elbow containing the effect of yield to tensile strength (Y/T) ratio. By non-linear regression analysis, available experimental data between the strain hardening exponent and Y/T ratio were fitted to mathematical models with high values of correlation coefficients. Meanwhile, in order to reflect the effect of different yield criteria on the burst pressure, the unified yield criterion is used and an analytical solution of burst pressure expressed as a function of parameter b, Y/T ratio, curvature impact factor and the ratio of thickness to radius is ultimately derived. Comparison with traditional theoretical results and numerical results show that the present Mises results considering the effect of Y/T ratio match the best with numerical results.

Etim Udoetok [26] developed equations to express the influence of internal fluid flow on the natural frequency and displacement amplitude of vibrating pipes. The approach involved complex mechanics and geometric analysis to arrive at new and simple equations which compares favourably with experimental results. The proposed new equations can be widely used to check and limit flow induced vibration level. More light is shed on the phenomena of steady internal fluid flow exacerbating the vibration of pipelines and piping systems. Sun-Hee et al [27] performed in situ tests for 664 days to measure deflections of buried GRP pipe with a large diameter of 2,400 mm. Based on the field test result, finite element analysis was conducted to determine the pipe deflections with respect to the soil conditions and buried depth as variables. Regression analysis were conducted to determine the long-term deflection of the GFRP pipe after 50 years of construction. Ana et al [28] presented experimental results conducted on three samples of a PN SN10000 DN150 PN10 pipe buried in three different types of terrain: neutral, acidic, basic. They were subjected to axial load, measuring the force applied deformation force function. On the basis of the calculation formulas determined rigidity of the pipeline, the deformation speed of 50 mm / min. Their conclusions show that the type of land affects the rigidity of the pipe, therefore, its length of life decreases to that provided by suppliers. Rita et al [29] in their work, presented the principal tools of the PIPE program developed to provide a friendly graphical user interface for the ANSYS software to perform finite element analyses of pipes with multiple rectangular defects in arbitrary position. The code allows a quick solid modelling, a guided non-linear analysis to obtain the failure pressure and also an error estimation to carry out a mesh refinement strategy. Error and burst analyses were carried out and experimental, numerical, and assessment methods results were compared. Ali et al [30]

DOI: 10.31695/IJASRE.2022.8.11.11

developed a thermosetting infield liner (IFL) using glass epoxy in response of the need for an optimized cost repair method. A burst test was conducted using ASME 106 steel pipes to measure their burst pressure which was later used to measure the performance of the thermosetting IFL. Three specimens were prepared for the burst test using a custom made burst rig. The burst pressure obtained was on average 245 bar of pressure. A numerical simulation was also conducted using ANSYS to create a validated model for future use in developing the thermosetting IFL. The results of the simulation show a 7% difference with the experiment results.

The focus of the study is to model the dynamic stability of the GRP pipe under specified flow conditions, using AWSYS software for model analysis, coming out comparative analysis of GRP pipes and that of ductile iron pipe and also using COMSOL multi-physics for fluid flow simulation through selected cases of straight, L and T shape.

1. Dynamic System Fluid Flow Modelling

Figure 1: A Clamped-Clamped Pipe Distribution

Considering the clamped-clamped distribution pipe with fluid flow resulting to vibration or disturbance of the membrane as a result of fluid impact or collision with the pipe wall and recirculation[17]. The dynamics of the system can be described by a partial differential equation:

$$q_4 \frac{\partial^4 y}{\partial x^4} + q_3 \frac{\partial^3 y}{\partial x^3} + q_2 \frac{\partial^2 y}{\partial x \partial t} + q_1 \frac{\partial^2 y}{\partial t^2} = 0 \qquad (1)$$

The pipe under consideration is of finite length, straight, clamped-clamped with fluid flowing through it. For this study, the following assumptions are considered:

- The finite pipe is placed horizontally
- The pipe is inextensible
- Shear strain, gravity and the coefficient damping material are ignored

Unlike most studies, the velocity distribution will not be ignored but rather, the dynamics relationship will be coupled with the Navier Stokes equation. However, for a pre-stressed pipe based on the beam theory the dynamic relation is given as:

$$EI \frac{\partial^4 y}{\partial x^4} + m_p \frac{\partial^2 y}{\partial t^2} = f_{\text{in}} \qquad (2)$$

Here, f_{in} is the inside force acting on the pipe, m_p is the pipe mass per unit length (kg/m) while EI is the bending stiffness of the pipe in Nm^2. For the internal fluid flow, an approximate internal force expression for a turbulent profile is given by equation (3)

$$f_{\text{in}} = -m_{fluid} \left. \frac{d^2 y}{dt^2} \right|_{x=U} \qquad (3)$$

Using local acceleration, Coriolis and centrifugal components of the acceleration to represent the total acceleration as expressed:

$$m_{fluid} \left. \frac{d^2 y}{dt^2} \right|_{x=U} = m_{fluid} \left[\left. \frac{d}{dt} \left(\frac{\partial y}{\partial t} + \frac{\partial y}{\partial x} \frac{\partial x}{\partial t} \right) \right|_{x=U} \right] = m_{fluid} \left[\left. \frac{d}{dt} \left(\frac{\partial y}{\partial t} + u \frac{\partial y}{\partial x} \right) \right|_{x=U} \right] = m_{fluid} \left[\frac{\partial^2 y}{\partial t^2} + 2u \frac{\partial^2 y}{\partial x \partial t} + u^2 \frac{\partial^2 y}{\partial x^2} \right] \qquad (4)$$

In addition, the flowing internal fluid exerts hydrostatic pressure on the pipe wall denoted as P_i and the corresponding force is $-A_i P_i$. Combining all these, Equation (3) can be comprehensively written as:

$$EI \frac{\partial^4 y}{\partial x^4} + \left(m_f u^2 - T \right) \frac{\partial^2 y}{\partial x^2} + 2 m_f u \frac{\partial^2 y}{\partial x \partial t} + \left(m_p + m_f \right) \frac{\partial^2 y}{\partial t^2} = 0 \qquad (5)$$

DOI: 10.31695/IJASRE.2022.8.11.11

For the pipe, the internal pressures results from the fluid flow hence, the dynamic equation will be coupled with fluid equations such as the momentum and continuity equation.

$$\frac{\partial \rho}{\partial t} + div \rho V = 0 \tag{6}$$

$$\rho \frac{DV}{Dt} = -\nabla p + \nabla \tau_{ij} + \rho g \tag{7}$$

2.1 Meshing of Fluid Volume and Boundary Condition

The meshing or discretization of the fluid volume (internal volume) of the geometries under consideration was generated using free tetrahedral mesh in *COMSOL Multiphysics*. Noting that both the GRP and ductile iron have the same internal diameter, fluid volume for both materials will be the same for equal pipe lengths. The straight pipe complete mesh consists of 8015134 domain elements, 188040 boundary elements, and 1090 edge elements. The elbow-joint complete mesh consists of 2903413 domain elements, 81288 boundary elements, and 1032 edge elements. Lastly, the T-joint complete mesh consists of 4232242 domain elements, 119378 boundary elements, and 1343 edge elements.

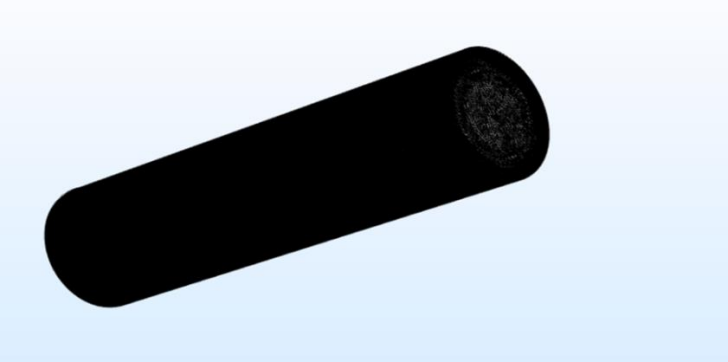

Figure 2: Fluid volume for the straight pipe

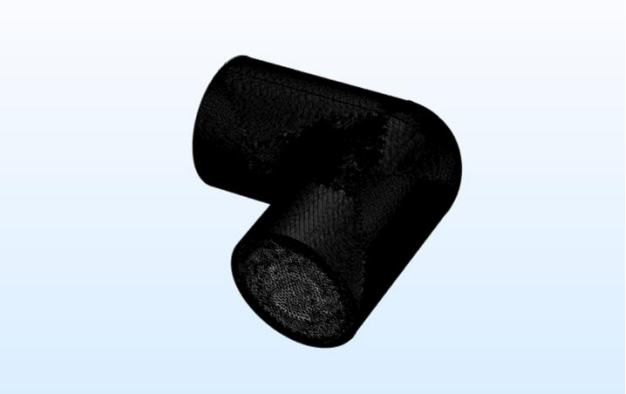

Figure 3: Elbow joint fluid volume

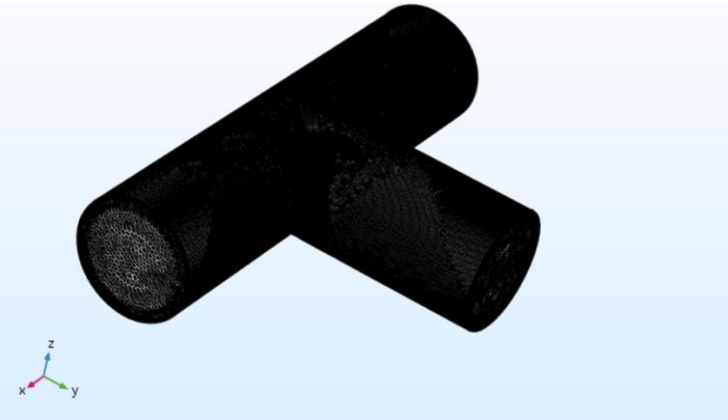

Figure 4: Fluid volume for the T-joint

DOI: 10.31695/IJASRE.2022.8.11.11

However, considering the straight pipe to be clamped-clamped at its end boundaries, the applicable boundary conditions of the pipe for the structural stability are given as:

$$y(0,t)=0 \qquad \frac{\partial^2 y(0,t)}{\partial t}=0 \tag{8}$$

$$y(L,t)=0 \qquad \frac{\partial^2 y(L,t)}{\partial t}=0 \tag{9}$$

Furthermore, for the fluid flow using water as a case study, the normal operating pressure range for water pipelines is 350 kPa to 550 kPa as given by Saskatchewan Environment pipe design guidelines. As a result, all the outflow pressure conditions used in the computation for the three geometries is 550kPa to account for the maximum pressure effect on the wall. The fluid flow velocities in water systems should not exceed certain limits to avoid noise and damaging of pipes and fittings. The table below can be used as a guide to maximum velocities T P Sathishkumar et al [31]:

Table 1: Data used for simulation

Application	Maximum Velocity (m/s)	(ft./s)
Tap water (low noise)	0.5 - 0.7	1.6 – 2.3
Tap water	1.0 - 2.5	3.3 – 8.2
Cooling water	1.5 - 2.5	4.9 – 8.2
Suction boiler feed water	0.5 – 1.0	1.6 – 3.3
Discharge boiler feed water	1.5 – 2.5	4.9 – 8.2
Condensate	1.0 – 2.0	3.3 – 6.5

From the Table 1, 3m/s is the maximum flow velocity. As a result, it was used as the normal inflow velocity. For material size of 10 inches which corresponds to class thickness of 50 and 59 for ductile iron and GRP respectively. The resulting Reynolds number at 20^0C (with density and dynamic viscosity of 998kg/m^3 and 1e-3kg/ms respectively) is given:

$$R_{eDi} = R_{eGRP} = 76e4 \tag{10}$$

From Reynold's number value, a turbulence model is appropriate for the work.

Raphael et al [17]. ASME B31G and modified ASME B31G simplify a short longitudinal corrosion defect as a parabolic curve whereas long corrosion defect can be simplified to a rectangular shape. According to ASME B31G and DNV-RP-F101 codes, the failure of corroded pipelines is controlled by the defect size as well as the flow stress of the material. The DNV-RP-F101 code can be applied for both defect subjected to internal pressure loading only or internal pressure loading combined with longitudinal compressive stresses. However, the ASME B31G is limited to defect subjected to internal pressure only. DNV-RP-F101 design code equations also include the assessment of single and interacting defects and complex shaped defects. C Cheng et al [18]. The input parameter of these codes include outer diameter of the pipe, D, wall thickness, t, yield strength of the material, σ_y or ultimate tensile strength, σ_u, the length of the defect, L and defect depth, d. The width, w is considered to have less effect on strength of corroded pipe and therefore this factor is avoided in all assessment equations N A Alang et al [3]. The equations used to calculate the burst pressure, Pb based on these codes are expressed as:

$$P_b = \frac{2tS_f}{D} \tag{10}$$

For ASME B31G:

DOI: 10.31695/IJASRE.2022.8.11.11

$$S_f = 1.1\sigma_y \left[\frac{1-\frac{2}{3}\left(\frac{d}{t}\right)}{1-\frac{\frac{2}{3}\left(\frac{d}{t}\right)}{M}}\right] \quad (11)$$

Where $M = \left(1 - 0.8\frac{L^2}{Dt}\right)^{0.5}$ (12)

For Modified ASME B31G:

$$S_f = \left(\sigma_y + 69\right)\left[\frac{1-0.85\left(\frac{d}{t}\right)}{1-\frac{0.85\left(\frac{d}{t}\right)}{M}}\right] \quad (13)$$

Here,

$$M = \left[1 + 0.6275\frac{L^2}{Dt} - 0.003375\left(\frac{L^2}{Dt}\right)\right]^{0.5} \quad (14)$$

For DNV-RP-F101:

$$S_f = \left(\sigma_y + 69\right)\left[\frac{1-0.85\left(\frac{d}{t}\right)}{1-\frac{0.85\left(\frac{d}{t}\right)}{M}}\right] \quad (15)$$

Where $M = \left[1 + 0.31\left(\frac{L^2}{Dt}\right)\right]^{0.5}$ (16)

M represents bulging stress magnification factor.

2.2 Von Mises Yield Criterion

Based on the Von Mises criterion, the yielding of the pipe wall will take place when the distortion energy reaches a certain limit value $\sigma_{von\ Mises}$ CKI Sung [19] This can be shown as in Equation (17).

$$(\sigma_h - \sigma_l)^2 + (\sigma_l - \sigma_r)^2 + (\sigma_r - \sigma_h)^2 = \sigma_{von\ Mises} \quad (17)$$

The value $\sigma_{von\ Mises}$ is obtained from the tensile test. In the case, $\sigma_h = \sigma_r = 0$ and $\sigma_l = F/A$, is the ratio of the applied tensile force F to the metal area A. In fact, yielding will take place when $\sigma_l = Sy$, where the von Mises criterion can be written as in Equation (18)

$$\left(0 - S_y\right)^2 + \left(S_y - 0\right)^2 + (0 - 0)^2 = \sigma_{von\ Mises} = 2S_y^2 \quad (18)$$

By substitution, the internal pressure at which the pipe wall yields is as shown in Equation (19)

$$P_y = \frac{S_y}{\sqrt{\frac{3}{4}\left(\frac{D}{2t}\right)^2 + \frac{3}{2}\left(\frac{D}{t}\right) + 1}} \quad (19)$$

P_y is the internal pressure at onset of yield, psi. For thickness ratio $\frac{D}{t} \gg 1$,

$$P_y = \frac{4tS_y}{D\sqrt{3}} \quad (20)$$

As the internal pressure continues to increase beyond the yield pressure, P_y the pipe wall will bulge outward and reach a point of instability. Actually, in reality the material is not perfectly uniform and this bulging does not take place exactly uniformly around the circumference but preferentially on the side of the pipe wall. The strain at which instability occurs is as shown in Equation (21):

$$\varepsilon_i = \frac{n}{2} \quad (21)$$

ε_i is the strain at onset of instability, and n is the strain coefficient.

After the instability, which is the outward bulge in pipe wall, the pipe ruptures. The pressure at rupture is the ultimate

DOI: 10.31695/IJASRE.2022.8.11.11

pressure P_u given as in Equation (22):

$$P_u = \left(\frac{2kt}{D}\right) e^{-n} \left\{ \frac{n}{\left[2\left(\frac{3}{4}\right)^{\frac{(1+n)}{n}}\right]} \right\}^n \quad (22)$$

Where t is the pipe thickness, in, k is the strength coefficient, psi, D is the pipe diameter, in.

Burst pressure for direct definition is; maximum pressure. To be general, a defective pipe would have a lower burst pressure rather than a non-defective pipe. To be précised, it is a pressure limitation of a pipe can withstand before it damage/defective

(without bursting). Burst pressure can be calculated by using Barlow's Formula

$$P = \frac{2st}{DSF} \quad (23)$$

Where s is the material ultimate tensile strength (MPa), t is the thickness of the pipe (mm), D is the internal diameter (mm) and SF is the safety factor. Equation (23) is based on ideal condition at room temperature with no defect on the pipe outer surface. Thus, ultimate tensile strength can be used to determine the bursting pressure and yield strength can be used at which the permanent deformation of the material begins. Zulfadli et al [20].

The ANSYS FEA software package has three different element types that can be used to model a pipe geometry with varying degrees of accuracy namely (i) BEAM189 (ii) PIPE288 (iii) PIPE289. The PIPE289 element was used to model the pipe geometry in this study because of its advantages over the BEAM189 and PIPE288. PIPE289 being a quadratic three-node pipe element in 3-Dimension based on Timoshenko beam theory which accounts for shear-deformation effects and stress stiffness terms. This makes the elements suitable for analysing flexural, lateral and torsional stability problems A Pati [32]. Figure 3.5 shows the finite element model of the pipe geometry as modelled in ANSYS R19.0.

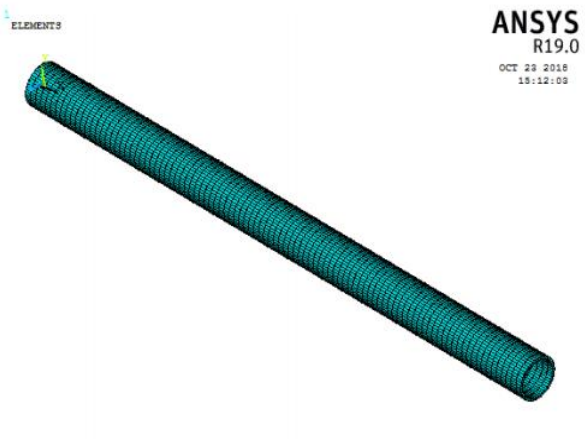

Figure 5: Finite Element Model of Pipe Geometry

2.3 Model Parameters

The parameters used in the modelling are: pipe inner diameter d, pipe thickness t, Young's modulus of elasticity of pipe material E (assumed directionally invariant for the GRP material), and density of pipe material. Table 2 presents model parameters and properties of materials used.

Table 2: Property and Parameter values for the model[30]

Property/Parameter	GRP Pipe	Ductile Iron Pipe
Inner Diameter, d	254mm	254mm
Thickness	1.07mm	6.35mm

DOI: 10.31695/IJASRE.2022.8.11.11

Density	1820kg/m^3	7086.56kg/m^3
Modulus of Elasticity	170GN/m^2	200GN/m^2

3. VALIDATION OF RESULTS

Being that the current study has no exact replica that could be used for validation; we will be validating the result using the existing and established expressions that has been proven to satisfy real life working conditions [33]. For this validation the Boardman and Lame´s theories will be used, which are bursting pressures expressions respectively.

$$P = \frac{2St}{D-(0.8t)} \quad (24)$$

$$P = \frac{S(D^2-d^2)}{(D^2+d^2)} \quad (25)$$

Using the equations (24) and (25) for both the GRP and ductile iron pipe bursting pressure for an internal diameter pipe of 254mm, Ultimate Tensile Strength of 4890Mpa for GRP and 827.4Mpa for ductile iron pipe to express the bursting pressure over a thickness range of 2mm $\leq$ t $\leq$ 20mm. In addiction using a factor of safety of 4.5, the workable pressures are also expressed graphically for both GRP and ductile iron pipes.

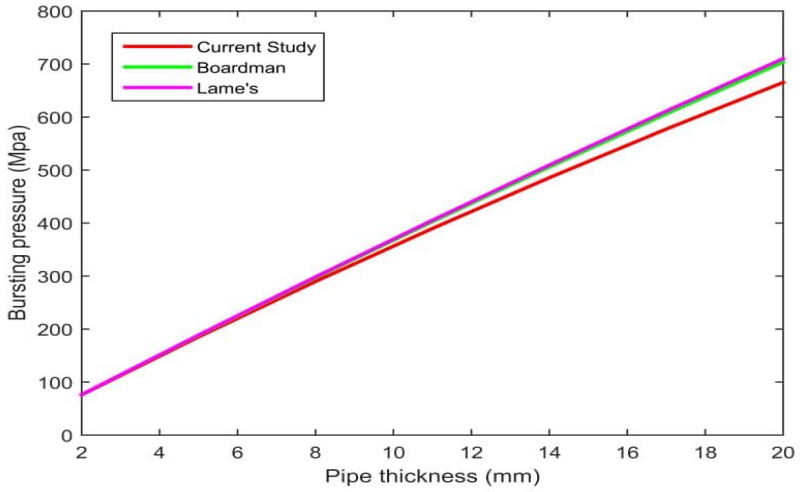

Figure 6: Bursting pressure versus the thickness using current study, Boardman and Lame´s established expression considering ductile iron pipe.

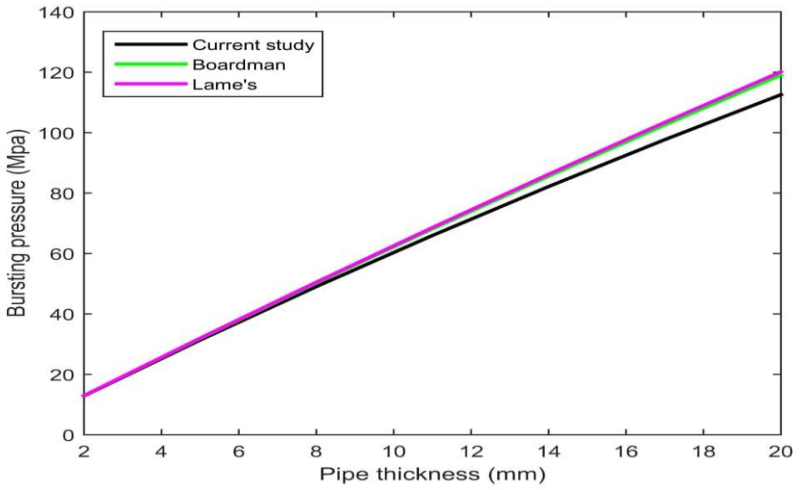

Figure 7: Bursting pressure versus the thickness using current study, Boardman and Lame´s established expression considering GRP pipe.

DOI: 10.31695/IJASRE.2022.8.11.11

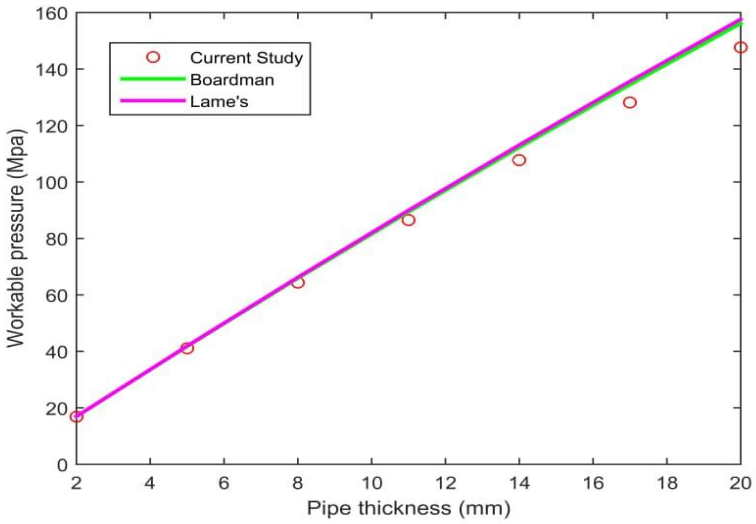

Figure 8: Workable pressure versus the thickness using current study, Boardman and Lame´s established expression considering ductile iron pipe.

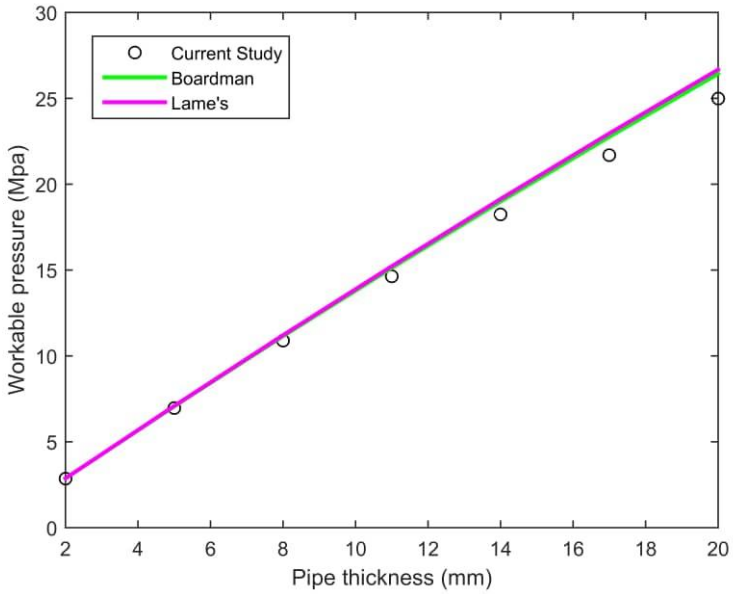

Figure 9: Workable pressure versus the thickness using current study, Boardman and Lame´s established expression considering GRP pipe.

It is practically observed that Lame and Boardman´s agreed over the pipe thickness range plotted. However, the current study deviates from both Boardman and Lames results for both bursting and workable pressures and it is visible from thickness above 10mm. For the bursting pressure the maximum percentage deviation of the ductile iron pipe and the GRP are 4.167% and 3.571% respectively.

3.1 Model Validation of Fluid Flow Simulations

To validate the accuracy and reliability of the models developed for the simulation, the error plot for all the three simulations were generated for each of the flow scenarios. The relative error for all the scenarios were less than ≤ 0.01. The Error plot for all the three flow scenarios (Straight pipe, elbow joint and T-joint) are shown in figures 10, 11 and 12. All the simulations did show reasonably low levels of error, which validates the reliability of the results of the simulations.

DOI: 10.31695/IJASRE.2022.8.11.11

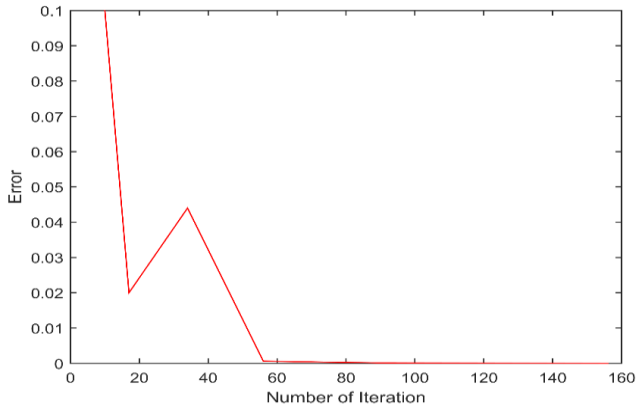

Figure 10: Relative Error for the Flow in a Straight Pipe

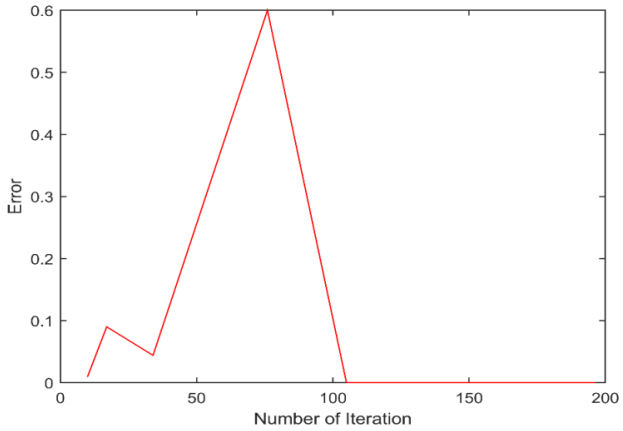

Figure 11. Relative Error plot for flow through the elbow joint

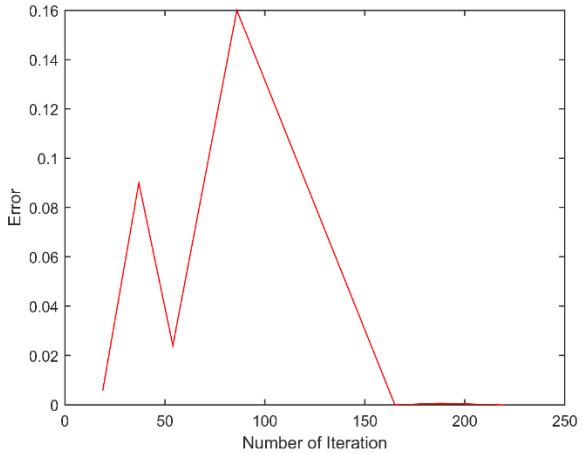

Figure 12: Relative Error Plot for flow through the T-joint

4. RESULTS AND DISCUSSION

Table 3: Lateral Deformation and Mode Shape.

Mode	DI	GRP
1	8.4314	9.6732
2	8.4967	9.6732
3	7.9739	9.1503
4	8.0392	9.1503
5	8.0392	9.1503

DOI: 10.31695/IJASRE.2022.8.11.11

6	7.9739	9.1503
7	11.8301	8.6928
8	7.6471	9.2157
9	8.0392	9.2157
10	8.0392	17.5163

Table 3 shows that lateral deformation of both GRP and DI pipes remain fairly constant with GRP pipe having higher values per mode shape for the first six mode shapes. The outliers are values for the bursting modes which are mode 7 for DI pipe and mode 10 for GRP pipe.

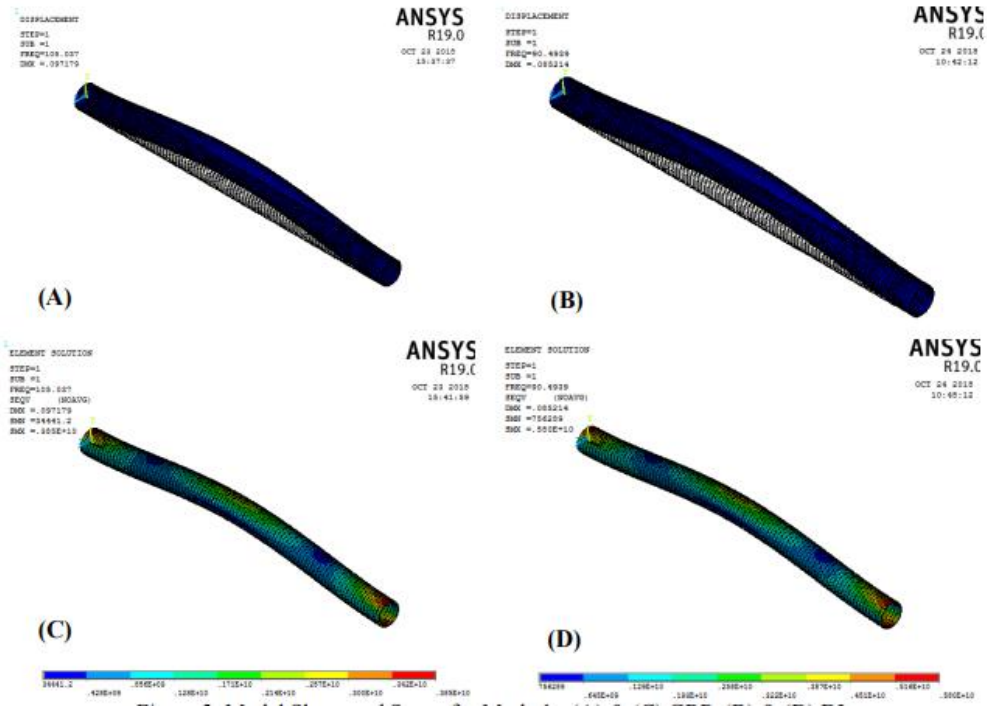

Figure **13. Model Shape and Stress for Mode 1 (A) and (C) GRP, (B) and (D) DI**

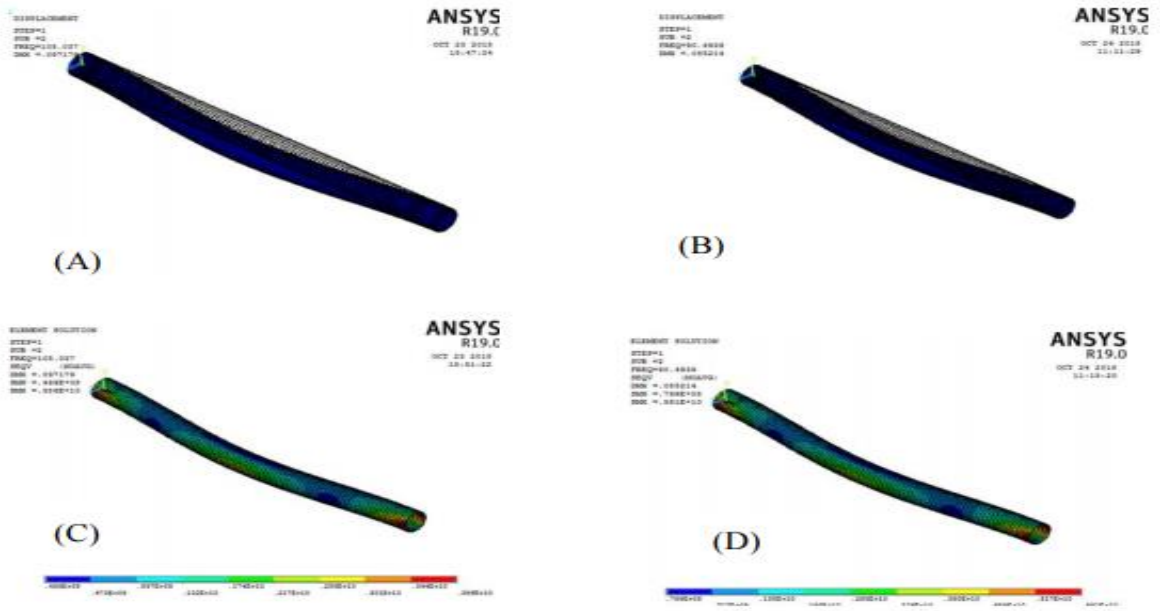

Figure 14: Modal Shape and Stress for Mode 2 (A) and (C) GRP, (B) and (D) DI

DOI: 10.31695/IJASRE.2022.8.11.11

Figures 13 and 14 show mode shapes 1 and 2 and they indicate the buckle type of mode shape for mode 1 and mode 2. The different deformation orientations in figure 13 are oriented in the y-axis showing an upheaval buckling while figure 14 shows deformations oriented in the x-axis showing a lateral buckling or snaking. The plots A and B show the model shape and frequencies of both GRP pipe and Ductile Iron pipe while plots C and D shows the equivalent Von Misses stresses of GRP pipe and Ductile Iron pipe. It is observed that for both modes, GRP pipe experienced more deformation and stress at higher frequency than Ductile Iron pipe.

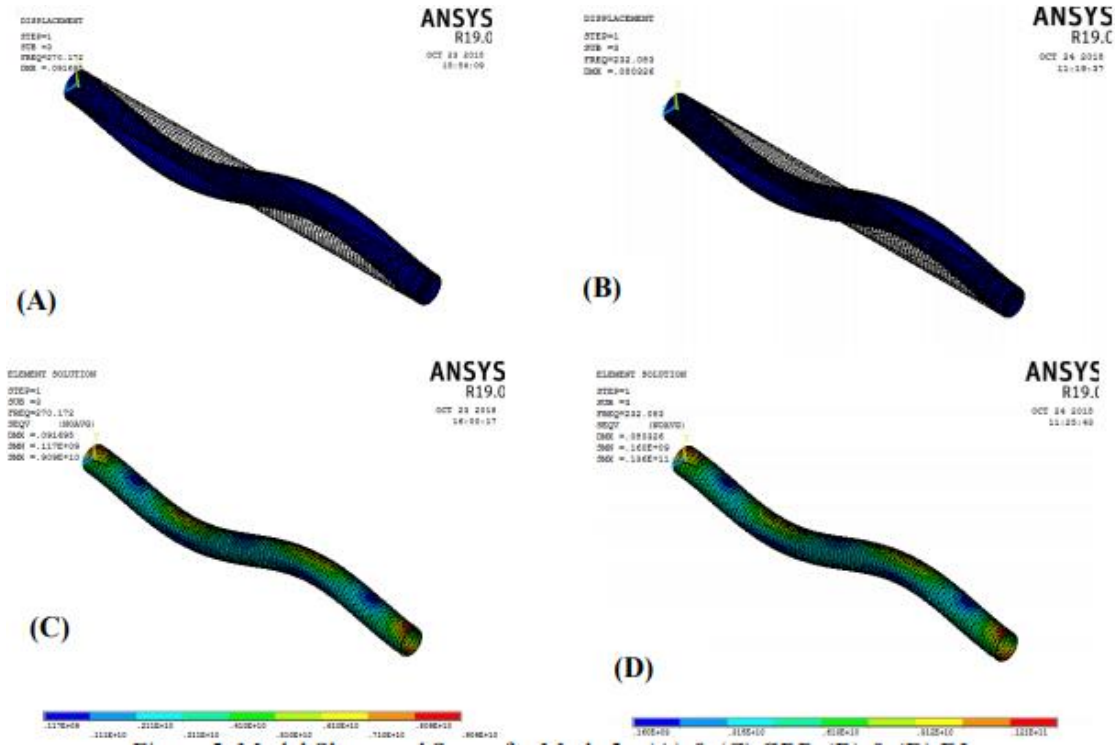

Figure 15: Model Shape and Stress for Mode 3 (A) and (C) GRP, (B) and (D) DI

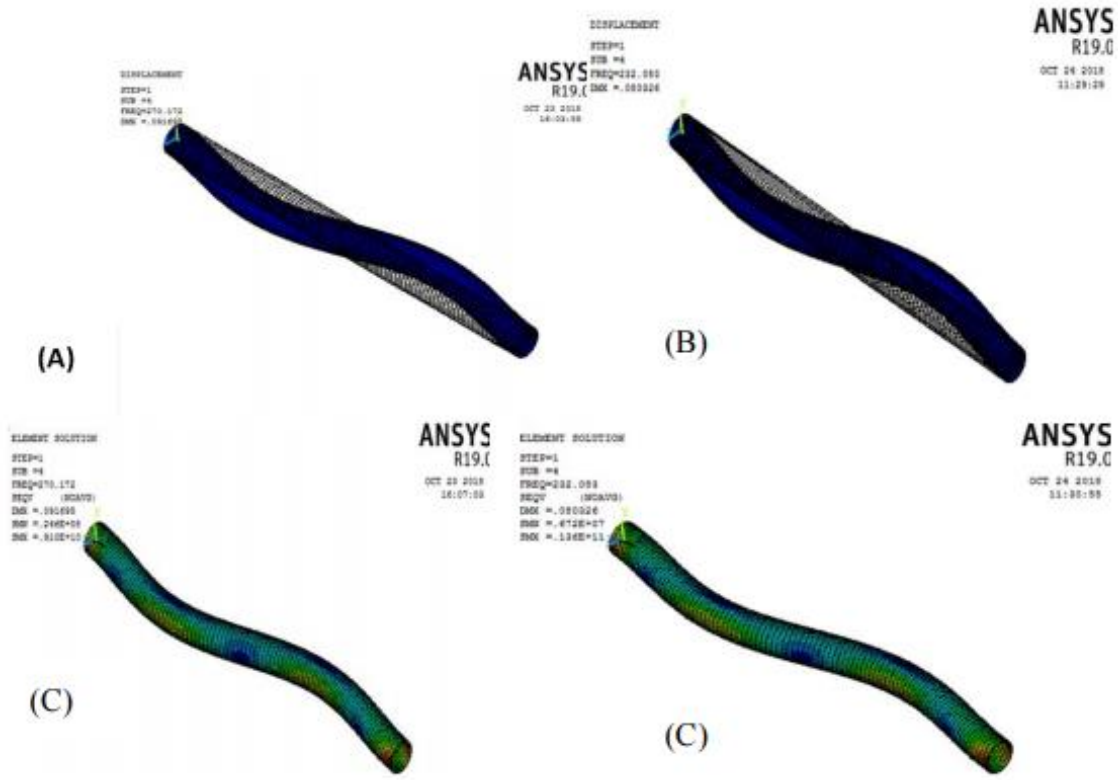

Figure 16: Model Shape and Stress Mode 4 (A) and (C) GRP, (B) and (D) DI

DOI: 10.31695/IJASRE.2022.8.11.11

For mode 3 and mode 4 as shown in figure 15 and figure 16, the figures indicate the buckle type of mode shape for mode 3 and mode 4, but different deformation orientations with figure 15 orienting in the y-axis showing an upheaval buckling while figure 16 orienting in the x-axis showing a lateral buckling or snaking. The plot A and B shows the model shape and frequencies of both GRP pipe and Ductile Iron pipe but the plot C and D shows the equivalent Von Misses stresses of GRP pipe and Ductile Iron pipe. It is observed that for both modes, GRP pipe experienced more deformation and stress at higher frequency than the ductile Iron pipe.

For mode 5 and mode 6 are shown in figure 17 and figure 18, the figures 17 and 18 indicates the buckle type of mode shape for mode 5 and mode 6, but different deformation orientations with figure 17 orienting in the y-axis showing an upheaval buckling while figure 18 orienting in the x-axis showing a lateral buckling or snaking. The plot A and B shows the model shape and frequencies of both GRP pipe and Ductile Iron pipe but the plot C and D shows the equivalent Von Misses stresses of GRP pipe and Ductile Iron pipe. It is observed that for both modes GRP pipe experienced more deformation and stress at higher frequency then Ductile Iron pipe.

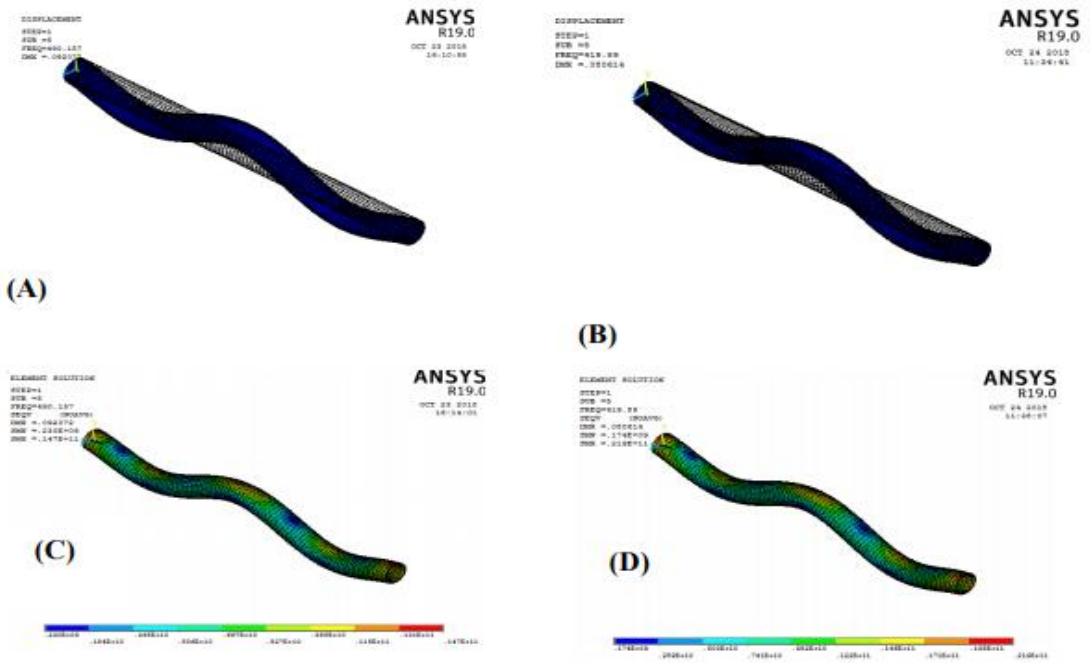

Figure 17: Model Shape and Stress Mode 5 (A) and (C) GRP, (B) and (D) DI

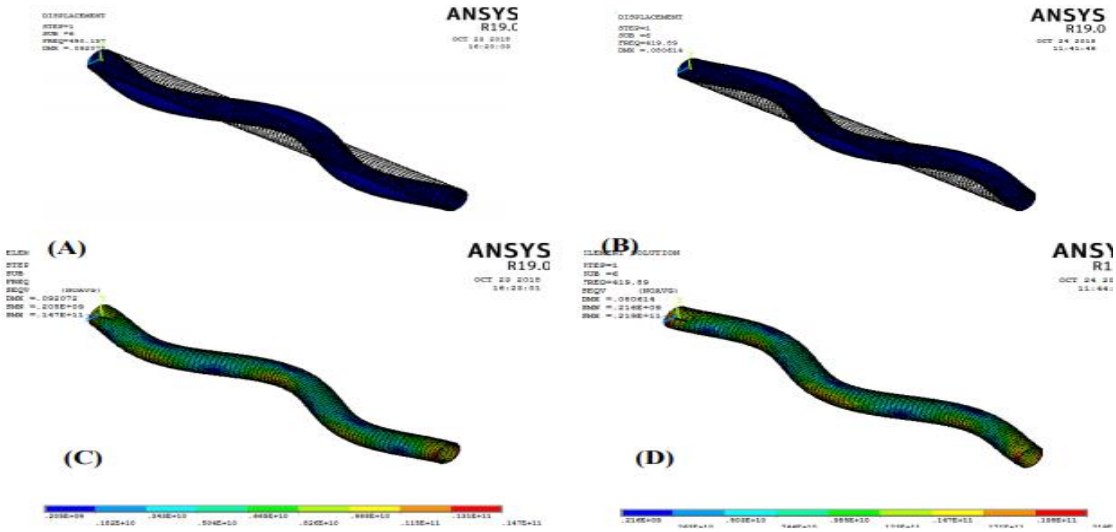

Figure 18: Model Shape and Stress Mode 6 (A) and (C) GRP, (B) and (D) DI

DOI: 10.31695/IJASRE.2022.8.11.11

Table 4. Values for Model Shape, Deformation, Stress Ratio and others.

S/N	MODE	DEFORMATION	EQUIVALENT VON MISES STRESS		STRESS RATIO	
		D.I GRP	D.I	GRP	D.I	GRP
1	1	8.4314 9.6732	5.7931	3.8621	0.0139	0.0410
2	2	8.4967 9.6732	5.7931	3.8621	0.0139	0.0410
3	3	7.9737 9.1503	13.6379	9.1724	0.0331	0.0387
4	4	8.0392 9.1503	13.6379	9.1724	0.0328	0.0387
5	5	8.0392 9.1503	21.8448	14.8448	0.0525	0.0390
6	6	7.9739 9.1503	21.9655	14.8448	0.0525	0.0363
7	7	11.8301 8.6928	19.7931	12.6784	0.0475	0.0369
8	8	7.6471 9.2157	19.3103	19.4310	0.0463	0.0393
9	9	8.0392 9.2157	28.8448	19.5517	0.0694	0.0393
10	10	8.0392 17.5163	28.9655	16.4438	0.0691	0.0741

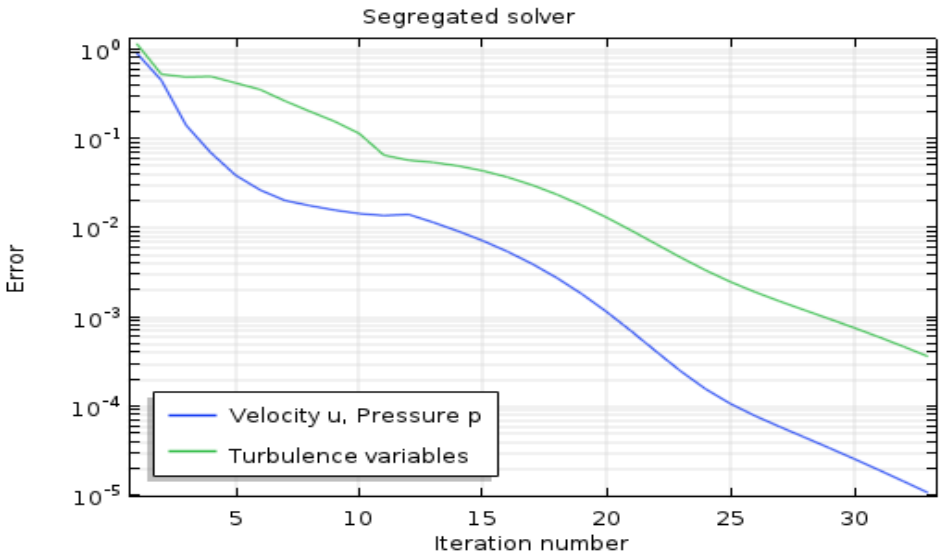

Figure 19: **The convergence plot of the simulation**

The convergence error at the end of the iterations is below 10^{-5}, which is considered small enough to produce reliable results.

DOI: 10.31695/IJASRE.2022.8.11.11

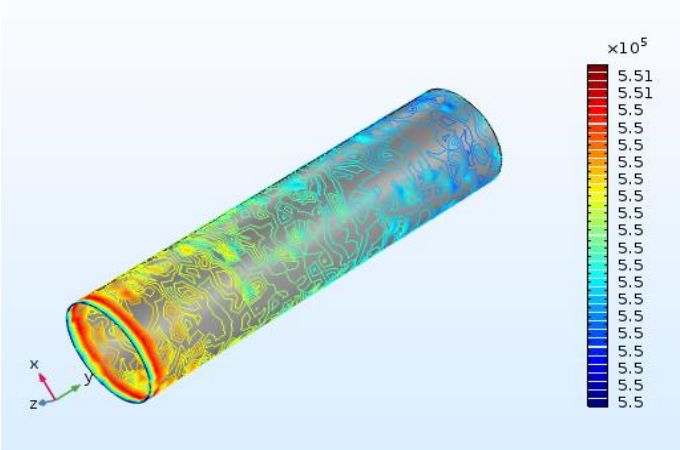

Figure 20: Fluid Flow Analysis and Pressure Contour for Straight Pipe

Figure 20 shows the fluid flow analysis and pressure contour for a straight pipe. The pressure profile shows that the maximum pressure experienced within the pipe occurs at the inlet with pressures in excess of 0.5 MPa. This pressure values are well below the bursting pressure of both GRP and ductile iron pipes.

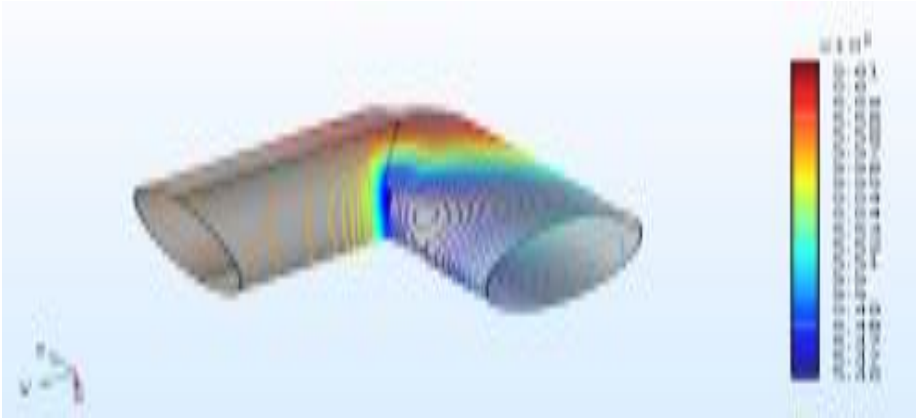

Figure 21. Flow Analysis and Pressure Contour for L-Shaped Pipe

Figure 21 shows the fluid flow analysis and pressure contour for L-shaped pipe. The pressure distribution shows peak pressures at the elbow, especially at the far end of the bend. The pressure values there are in excess of 0.56MPa. This peak pressure values are below the pipe bursting pressures for the GRP and ductile iron pipes.

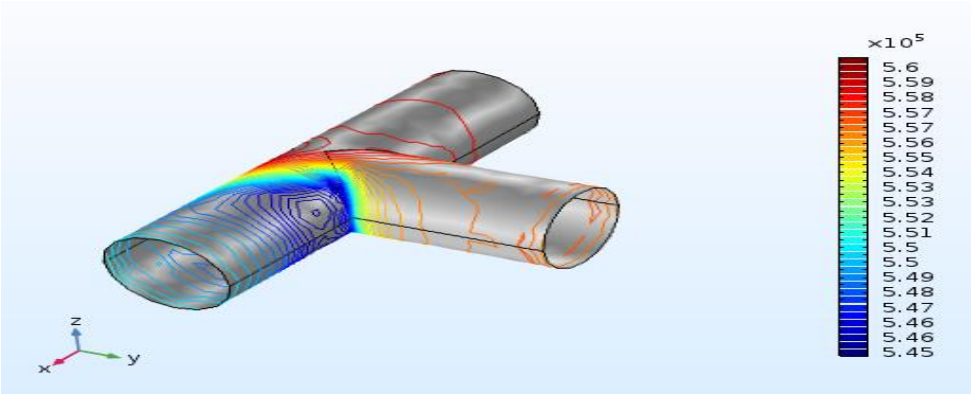

Figure 22: Flow Analysis and Pressure Contour for T-shaped

DOI: 10.31695/IJASRE.2022.8.11.11

Figure 22 shows the flow analysis and pressure contours for a T-shaped pipe. The pressure distribution across the pipe shows that the high pressure regions are around the inlet and culminates at the T-junction. The maximum pressure obtainable in this section is in excess of 0.56MPa. This pressure is less than the calculated bursting pressure of both GFRP and ductile iron pipe based on the

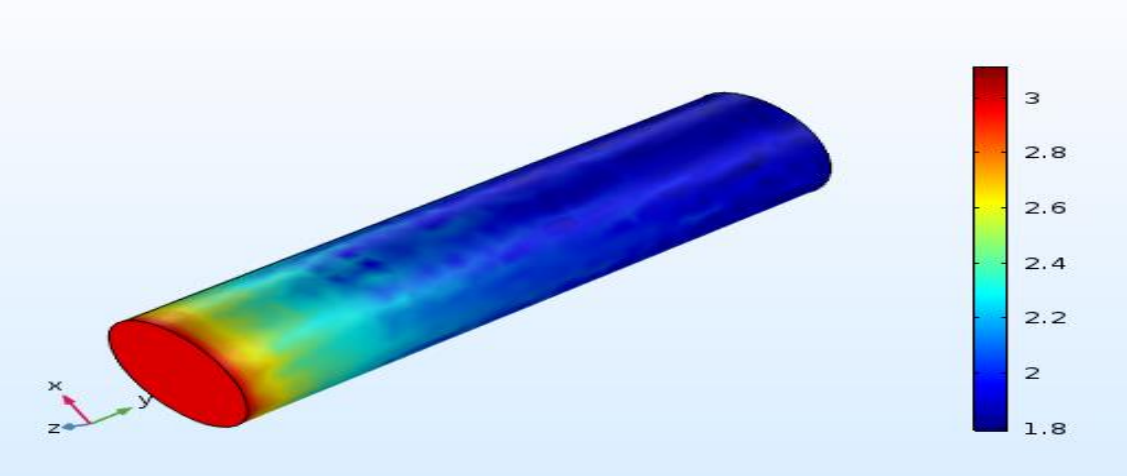

Figure 23: Flow Velocity Profile for the Straight Pipe

dimensions given in table 1. Figures 23 - 25 show the velocity distribution across the pipes, for the straight, L-shaped and T-shaped pipes. The highest velocities are observed at the inlets, and subside as flow progresses. The peak velocities were recorded in the L-shaped pipe which is approximately 5m/s.

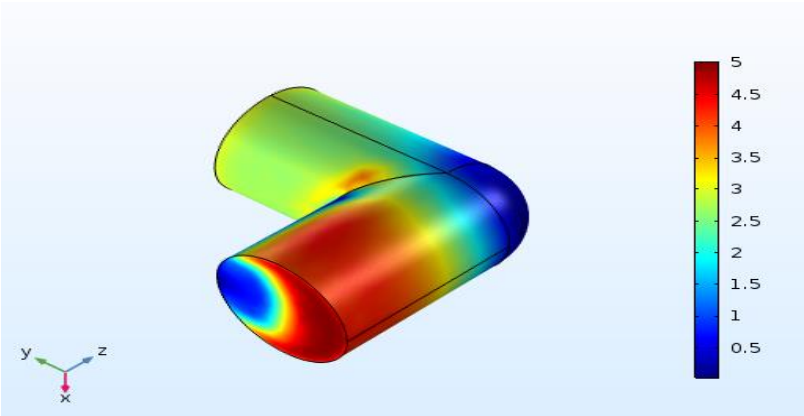

Figure 24: Flow Velocity Profile for L-shaped pipe

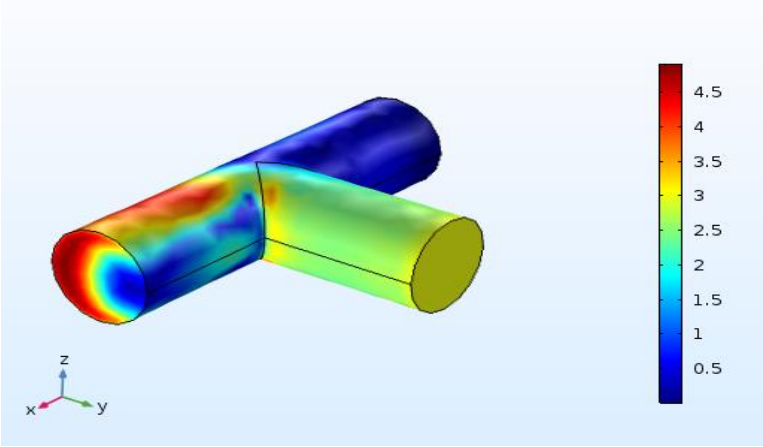

Figure 25: **Flow Velocity Profile for a T-Shaped Pipe**

The plots of the bursting pressure against pipe thickness, that of Bursting Pressure against thickness ratio and that of thickness versus thickness ratio for the GRP as compared to those of the DI for class 50 and 64 are shown in figure 26.

DOI: 10.31695/IJASRE.2022.8.11.11

International Journal of Advances in Scientific Research and Engineering (ijasre)

E-ISSN : 2454-8006

DOI: 10.31695/IJASRE.2022.8.11.11

Volume 8, Issue 11
November - 2022

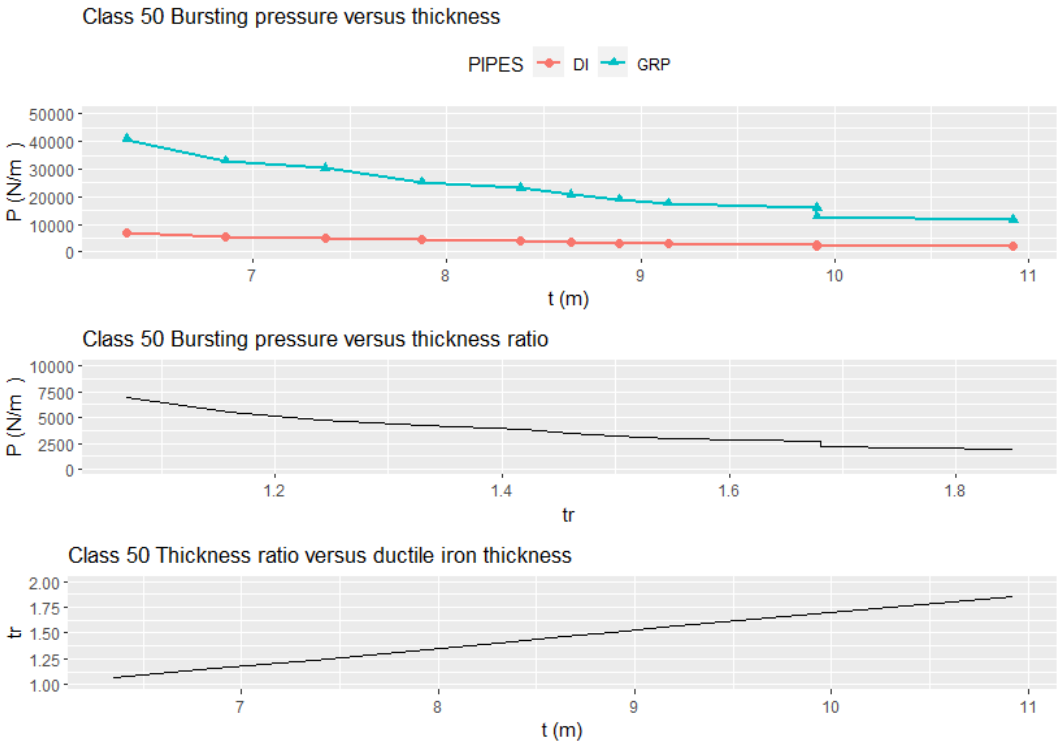

Fig 26: The plot of bursting pressure for class 50, thickness and thickness ratio

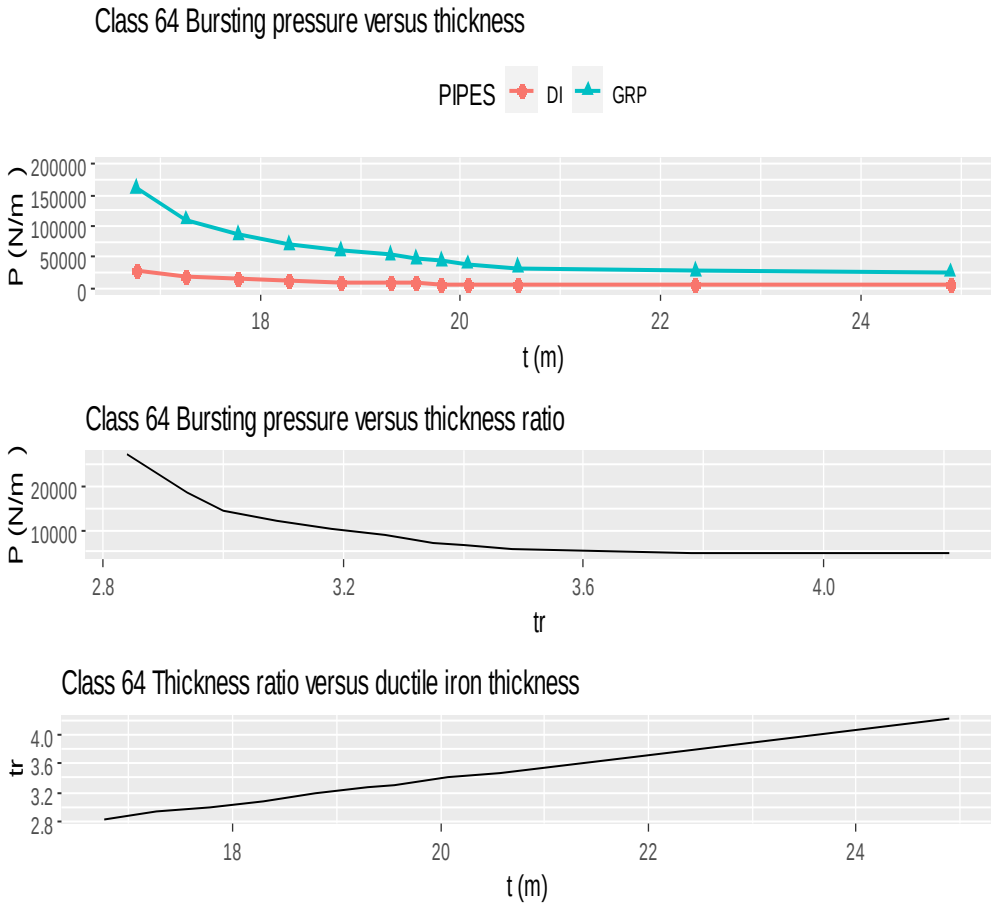

Fig .27: The plot of bursting pressure for class 64, thickness and thickness ratio.

6. CONCLUSION

It is common knowledge that Glass fibre reinforced polymers have high resistance to corrosion and erosive wear. This study however focuses on the internal flow of fluid through GRP pipes in comparison with the predominantly used ductile iron pipes. Since both pipes considered for this study are of the same internal dimension, it is safe to assume equal fluid volume. Subject to the flow conditions given, which according to literature and industrial applications, are the predominant flow conditions for water distribution channels, the maximum obtainable pressures within the channel for straight pipes are slightly above 0.55 MPa, 0.561MPa for L-shaped pipes and 0.56MPa for T-shaped pipes. The peak pressures obtained are all less than the pipe bursting pressure for both GRP and DI pipes for the given pipe dimensions. This is a pointer to the suitability of GRP pipes for water distribution applications. More so, from the table 4.3, the summary of the calculated pipe bursting pressures for the various classes of pipes show that GRP pipes have the capacity to withstand high pipe bursting pressures. It is therefore safe to say that GRP pipes are more recommendable for high pressure applications with respect to maintenance, corrosion and wear resistance.

For the model analysis performed for both pipe material types, six lateral vibration modes were identified as significant for both pipes bearing the property and parameter values for the mode chosen in mind. The comparative analysis of the performance of the different pipes show that for same mode shape numbers, GRP pipes experienced higher lateral deformation values and higher model frequencies. Harmonic frequency and von Mises stress were higher for GRP pipe than DI pipe. A significant insight into this shows that the stress ratio for GRP pipe is only higher than DI pipe for the first four modes. This suggests that GRP pipes of equivalent bursting strength as the DI pipe will perform better at applications prone to higher excitation frequencies. More so, it is also seen that GRP pipes undergo higher lateral deformations in nearly all modes except mode 7. The velocity distribution is as shown in figures 4.16-4.18. Peak velocities are expected in L-shaped pipes and in the neighbourhood of 5m/s.

Nomenclature

A	Cross sectional area of the body	M_1	Mass of fluid per unit length
D	Outside diameter	M_2	Mass of pipe per unit length
E	Modulus Elasticity	P	Load (Force)
EI	Flexural Rigidity	P_b	Bursting Pressure
I	Second Moment of Inertia	P_r	Internal pressure
M_1	Mass of fluid per unit length	R	Pipe inner radius
M_2	Mass of pipe per unit length	S	Material Ultimate Tensile Strength
P	Load (Force)	S_h	Hoop Stress
P_b	Bursting Pressure	t	Pipe wall thickness
P_r	Internal pressure	T_m	time
R	Pipe inner radius	U	Axial mean velocity
S	Material Ultimate Tensile Strength	u	Velocity fluctuation in x direction.
A	Cross sectional area of the body	V	velocity fluctuation in the y direction.
D	Outside diameter	Va	Azimuthal mean velocity
E	Modulus Elasticity	X	Axial Co – ordinate
EI	Flexural Rigidity	Y	Distance from the pipe centre normal to the fin leading edge.
I	Second Moment of Inertia	ϵ	Strain
		σ	Stress

DOI: 10.31695/IJASRE.2022.8.11.11

REFERENCE

[1] M. Zulfadli and B. I. N. Mohamad, "Determination of Bursting Presure of Defective Steel pipes," *Proj. report, Univ. Malaysia, Pahang*, no. June, 2012.

[2] P. Sonny, "Spatial Modelling of Water Pipe Bursts in Harare ," *Masters Diss.*, no. June, 2008. University of Zimbabwe, Faculty of Science, Department of Geography.

[3] M. S. A. majid and R. D. Z. S. Nazirah, "Effects of elevated temperatures on glass-reinforced epoxy pipes under multi-axial loadings," *J. Mech. Eng. Sci.*, vol. 10, no. 1, pp. 1846–1856, 2016.

[4] N. A. Alang, N. A. Razak, K. A. Shafie, and A. Sulaiman, "Finite Element Analysis on Burst Pressure of Steel Pipes with Corrosion Defects," in *13th International Conference on Fracture*, June 16-21,2013, Beljing ,China.

[5] A. Landesmann, C. A. Seruti, and E. D. M. Batista, "Mechanical Properties of Glass Fiber Reinforced Polymers Members for Structural Applications," *Mater. Res.*, vol. 18, no. 6, pp. 1372–1383, 2015.

[6] N. K. Thomas, S. P. George, S. M. John, S. George, and M. S. Steve, "Stress Analysis of Underground GRP Pipe Subjected to Internal and External Loading Conditions," *Int. J. Adv. Mech. Eng.*, vol. 4, no. 4, pp. 435–440, 2014.

[7] H. Shi, H. Yin, and L. Wei, "Model Test on Mechanical Properties of Glass Fiber Reinforced Plastic Mortar Pipes Culvert Under High Embankment," *Int. J. Performability Eng.*, vol. 14, no. 6, pp. 1352–1359, 2018.

[8] F. Lavergne,K Sab[a*] , J Sanahaja[b],M Bonnet[a]C Toulemonde[b] "Estimation of creep strain and creep failure of a glass reinforced plastic by semi-analytical methods and 3D numerical simulations," *Mechanics of Materials,Elsevier,2015,89,pp,130-150.10.1016/j.mechmat.2015.06.005.*

[9] M. A. Masuelli, "Introduction of Fibre-Reinforced Polymers − Polymers and Composites : Concepts , Properties and Processes,"DOI:10.5772/54629, *Intech open*, pp. 3–40, January 23, 2013.

[10] W. Jun, G. Hota', L. Ruifeng', Z. Ding, W. L. And, and Y. Fang, "Durability of glass fiber-reinforced polymer composites under the combined effects of moisture and sustained loads," *Journal of Reinforced Plasticand Composites.* vol. 34, pp. 1739–1754, July,2015.

[11] H. Shi, L. Wei, Y. Li, and R. Gao, "Laboratory evaluation on fatigue performance of glass fiber reinforced plastic mortar pipes culvert," *Rom. J. Mater.*, vol. 48, no. 3, pp. 388–393, 2018.

[12] Y. Yuan, C. Liu, and M. Huang, "The structure and performance of short Glass Fiber/High Density Polythene/ Polypropene Composite Pipes Extruded Using a shearing - Drawing component stress field," *MDPI*, 23 April, 2019.

[13] R. E. S. and R. J. Bishop, *Materials, Modern Physical Metallurgy and Engineering*, Sixth. Oxford: Butterworth-Heinemann, 1999.

[14] R. Jain and L. Lee, *Fiber Reinforced polymer (FRP) Composites for Infrastructural Applications*. New York: Springer, 2012.

[15] D. V. Rosato and D. V. Rosato, *Reinforced Plastics Handbook*, 3rd ed. Oxford: Elsevier Ltd, 2004.

[16] A. W. Abdel-ghany, I. Taha, and S. J. Ebeid, "Failure Prediction of Fiber Reinforced Polymer Pipes using FEA," *Innational Journal of Engineering and Technical Research(IJETR)*, vol. 0869, no. 2, pp. 115–120, 2016.

[17] H. Liu, "Revised Burst Model for Pipeline Integrity Assessment," Master's Thesis, Engineering Failure Analysis, volume 80, page 24 - 38, October 2017 .

[18] O. Raphael, O. Efosa, and E. Sylvester, "On the Dynamic Behaviour of Glass Fiber-Reinforced Plastic Pipe with Clamp- Clamp Boundary Condition," *Adv. Eng. Des. Technol.*, vol. 1, no. 1, pp. 1–12, 2019.

[19] C. Cheng and G. E. O. Widera, "Development of a Simplified Theoretical Model for Dynamic Burst Time And Pressure of a Cylindrical Shell," *Open Ocean Eng. J.*, vol. 2, pp. 1–6, 2009.

[20] C. K. I. M. Sung, "Prediction of Burst Pressure on Steel Pipes using Gurson-Tvergaard-Needleman (GTN) Model,"

DOI: 10.31695/IJASRE.2022.8.11.11

Project paper, University of Malasia, June, 2013.

[21] P. Vasilyev and L. Fromzel, "Analytical Study of Piping Flow-Induced Vibration . Example of Implementation .," in 17th International Conference on structural mechanics inn reactor technology, Prague, Czech Republic,August 17-22,2003.

[22] M. Siba, W. Wanmahmood, M. Z. Nuawi, R. Rasani, and M. Nassir, "flow-induced vibration in pipes : challengess and solutions - a review," *J. Eng. Sci. Technol.*, vol. 11, no. 3, pp. 362–382, 2016.

[23] X. Zhu and B. N. Leis, "Evaluation of burst pressure prediction models for line pipes," *Internertional Journals for presure vessels and piping,volume 89, pages 85 - 97. January,2012.*

[24] F. Yuan, L. Tsai, V. Prakash, A. Rajendran, and D. P. Dandekar, "Dynamic shear strength of S2 glass fiber reinforced polymer composites under shock compression," *Journal Appl. Phys.*,volume 103,May 29, 2008.

[25] S. H. Zhang, X.-D. Chen, X. Wang, and J.-X. Hou, "Modeling of burst pressure for internal pressurized pipe elbow considering the effect of yield to tensile strength ratio," *Meccanica*,50(8). August, 2015.

[26] E. S. Udoetok, "Internal Fluid Flow Induced Vibration of Pipes," *J. Mech. Des. Vib.*, vol. 6, no. 1, pp. 1–8, 2018.

[27] S. Kim, S. Yoon, and W. Choi, "Experimental Study on Long-Term Ring Deflection of Glass Fiber-Reinforced Polymer Mortar Pipe," *Adv. Mater. Sci. Eng.*, vol. 4, pp. 1–10, 2019.

[28] A. D. Ancas, M. Profire, I. L. Cirstolovean, M. Hornet, and G. Cojocaru, "lifetime glass reinforced plastic pipes by measuring the stiffness," *Journal of . Applied. Engineering. Science.*, vol. 8, no. 1, pp. 7–12, 2018.

[29] R. C. C. Silva, J. N. C. Guerreiro, and P. R. C. Drach, "Automatic finite element solid modeling , burst and error analyses of corroded pipelines," *Int. J. Mech.*, vol. 2, no. 3, 2008.

[30] A. Akram, Z. Mustaffa, and T. Albarody, "Numerical Simulation and Experimental Test on the Burst Pressure of ASME A106 Steel Pipe," in *ICCOEE*, 2018, vol. 06002, pp. 1–10,Malysia.

[31] T. P. Sathishkumar, S. Satheeshkumar, and J. Naveen, "Glass fiber-reinforced polymer composites – a review," *J. Reinf. Plast. Compos.*, vol. 33, no. 13, pp. 1258–1275, 2014.

[32] A. Patil, "Stress Analysis For GRP Piping Systems - Literature Review," *Int. Mod. Eng. Res.*, vol. 8, pp. 16–22, December, 2018.

[33] Meena Rezkallah (2014) ASME B-313 Presure Design of a straight pipe for internal presure.

[1] Email: empireObuh@yahoo.com

DOI: 10.31695/IJASRE.2022.8.11.11